Vision Res. Vol. 32, No. 7, pp. 1373–1393, 1992
Printed in Great Britain.

0042-6989/92 $5.00 + 0.00

Modeling the Dynamics of Light Adaptation: the Merging of Two Traditions

NORMA GRAHAM,* DONALD C. HOOD*

Received 12 August 1991; in revised form 11 December 1991

Light adaptation has been studied using both aperiodic and periodic stimuli. Two well-documented phenomena are described: the background-onset effect (from an aperiodic-stimulus tradition) and high-temporal-frequency linearity (from the periodic-stimulus tradition). These phenomena have been explained within two different theoretical frameworks. Here we briefly review those frameworks. We then show that the models developed to predict the phenomenon from one tradition cannot predict the phenomenon from the other tradition, but that the models from the two traditions can be merged into a class of models that predicts both phenomena.

Spatial frequency Temporal frequency Light adaptation Dynamics Background-onset effect High-frequency linearity

INTRODUCTION

The nervous system of higher animals, including humans, contains large sections dedicated to visual perception. In primates, in addition to the retina of each eye and a number of sub-cortical areas, a large portion of the cerebral cortex is also involved in processing visual information, perhaps as much as 25–40% in the case of humans (van Essen, 1985). Although we are far from a detailed understanding of how the nervous system performs the computations necessary for visual perception, a good deal of progress has been made. Over the last two decades, models have been suggested for visual processes that include relatively high-level processes such as the perceptual segregation of different regions in the visual field and the extraction of three-dimensional shape (for a sampling of a number of these, see Landy & Movshon, 1992).

Higher-level processes like these presumably occur in the cortex of primates. To make a model of these higher-level processes truly computable, it would be useful (and may be necessary) to have a satisfactory quantitative account of the processing that goes on at lower levels in the visual system. One very important lower-level process, thought to be primarily determined by retinal processing, is adaptation to different levels of light. Humans, for example, can adjust to ambient light levels that vary by a factor of 10^8 or more. Over much of this range, the visual system remains exquisitely sensitive to small differences in ambient light and the response to any given contrast remains approximately, but not exactly, constant. See reviews by Hood and Finkelstein (1986) and Shapley and Enroth-Cugell (1984). If this light-adaptation process is not properly modeled, it may be difficult to model any higher-level visual process satisfactorily since the input to that higher-level process will be poorly understood.

Are existing models of light adaptation good enough to serve in the formulation of models of higher-level processes? We examined candidate models that came from two traditions of investigation. The first and older tradition used aperiodic stimuli (e.g. dots and lines superimposed for a short period of time on backgrounds of different light intensity); the second and newer tradition used periodic stimuli (e.g. sinusoidally-flickering lights and spatially-sinusoidal gratings where the mean intensity of the sinusoids was systematically varied). The candidate models were chosen because they were successful at explaining the phenomena in the tradition in which they were developed. It was not clear, however, that the models would be successful at explaining the phenomena from the other tradition. In reviewing these models here, we focus on two empirical phenomena, one from each tradition and each as old as the tradition that spawned it: (i) the *background-onset effect* from the aperiodic tradition (a test's threshold is highest near the onset of a background light and then decreases) and (ii) *high-temporal-frequency linearity* from the periodic tradition (when amplitude sensitivity for flickering stimuli is plotted as a function of temporal frequency, there is a common high-frequency envelope for curves at different mean luminances). These phenomena emerged early in our work as particularly useful for diagnosing weaknesses of models.

As will be described below, none of the existing models from either tradition could account for the empirical phenomena from both traditions. It became clear, however, that judicious merging of various pieces of models from the two traditions could lead to a model that can account for a wide range of empirical results on light adaptation and which might, therefore, be good

*Department of Psychology, Columbia University, New York, NY 10027, U.S.A.

enough to serve in the formulation of models of higher-level processes.

Comment about multiple wavelength, spatial, and temporal channels

To reduce our review to manageable size, the models we discuss will only be compared to experimental results from photopic foveal vision. Further, the models examined will include only a single pathway or channel. In particular, we do not include multiple channels sensitive to different ranges of (electromagnetic) wavelength or of spatial frequency in spite of the fact that evidence for such channels is overwhelming. Indeed, the elegant work of Stiles on light adaptation was designed in part to explore the different channels sensitive to wavelength (e.g. Stiles, 1959). Less work has been done on the differential light adaptation of different spatial-frequency channels; some of it will be discussed briefly below. Because only a single channel is included in our models, the set of parameters specifying one of these models will probably apply only to stimuli of some particular wavelength and spatial-frequency content. If the set of wavelengths and/or spatial frequencies contained in the stimuli is altered, then, at the least, the values of the parameters specifying the model's single channel would be expected to change. More dramatically, the very structure of the channel might change.

The models we consider also include only a single temporal channel rather than multiple channels acting in parallel and sensitive to different ranges of temporal frequency. The justification for and implications of ignoring multiple temporal channels are somewhat different than those in the case of multiple wavelength and spatial-frequency channels. Although there is some psychophysical evidence for temporal-frequency selectivity, there is undoubtedly much less selectivity for temporal frequency than for spatial frequency or wavelength (see review in Chap. 12, Graham, 1989). Thus starting with a single temporal channel for simplicity is not too misleading even when one allows the temporal content of the stimuli to vary arbitrarily. This is important because our goal is to produce a computable model of light adaptation—that is, one which will predict the response to any arbitrary function relating variations in retinal illuminance to time.

THE APERIODIC-STIMULUS TRADITION

The use of aperiodic stimuli in investigations of light adaptation has a long history. Weber's law (the fact that the difference threshold ΔI is approximately proportional to the background intensity I for backgrounds of moderate to high intensity) may have its roots in the eighteenth century. [According to LeGrand (1957) this fact was discovered for vision by Bouguer (1760) but Weber extended it to many sensory modalities.] By the 1940s, Stiles had presented an explicit and well worked out quantitative model of adaptation designed to predict the threshold of a test spot for test and adapting stimuli of different intensities and wavelengths. Important in Stiles' work was the quantitative specification of sensitivity changes over a wide range of adapting intensities. Stiles' model did not, however, include time as a variable and thus did not attempt to predict the dynamics of light adaptation. These dynamics were, however, being extensively explored although not explicitly modeled (e.g. Craik, 1938; Crawford, 1947; Baker, 1949). A review of the aperiodic-tradition literature can be found in Hood and Finkelstein (1986).

Background-onset effect

In one of the most influential of these experiments on dynamics, Crawford (1947) measured the threshold for a brief test light presented before, during, and after the presentation of a larger background light (which he called the conditioning flash). He found that the test threshold was highest near the onset of the background light and that threshold decreased substantially over the next 200 msec or so. (Threshold increased again at the offset of the light. The effect at offset, although smaller, is interesting in its own right but will not be discussed here.) Subsequent work by Baker (1949) and Boynton and Kandell (1957) confirmed that threshold is highest at background onset. During the 1970s, a number of investigators compared the threshold at background onset to thresholds for test lights delayed relative to background onset (e.g. Alpern, Rushton & Torii, 1970; Shevell, 1977; Geisler, 1978; Hood, Ilves, Maurer, Wandell & Buckingham, 1978). These studies used a paradigm, called the probe-flash paradigm by Hood *et al.* (1978), that included a wide range of background intensities and was designed to study nonlinearities associated with light adaptation. Figure 1 shows data collected using conditions favoring foveal vision (Finkelstein, Harrison & Hood, 1990). In this figure, the threshold for detection of the test probe is plotted as a function of the intensity of the background light for two different delays between background onset and test probe onset (stimulus-onset asynchronies, abbreviated SOAs. When the background is presented as a steady light (SOA = ∞, solid circles), then the threshold of the test probe increased along a slope of approx. 1.0 (Weber's law). When the test probe is presented at the onset (SOA = 0, open circles in Fig. 1) of a background flash, however, the slope of the threshold vs illuminance (tvi) curve is greater than 1, usually between 1.5 and 2. Notice that the threshold at the onset of the background (SOA = 0) is always higher than the threshold for the same light upon a steady field (SOA = ∞). We will refer to the results illustrated in Fig. 1 as the *background-onset effect*.

This *background-onset effect* is the psychophysical phenomena from the aperiodic-stimulus tradition that we will compare to predictions from various models. Specifically, we will attempt to account for the two major features of the data in Fig. 1: the slope of the curves at higher intensities and the relative position of the curves. The SOA = 0 curve has a slope greater than 1 and sits to the left of the SOA = ∞ curve, which has a slope of about 1.

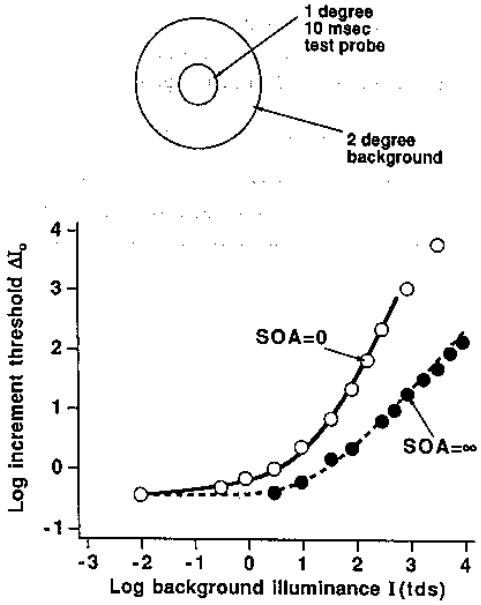

FIGURE 1. Background-onset effect. Log threshold intensity for a test stimulus as a function of log background intensity when the test comes on at the same time as the background (SOA = 0) or at a much later time (SOA = ∞). Points show data. Solid line is model prediction described in text. Modified from Finkelstein *et al.* (1990).

Static nonlinear models of adaptation from the aperiodic tradition

A theoretical framework coming from an aperiodic tradition is well able to account for this background onset effect, as we will see below. This approach was introduced by Geisler (1978, 1979) and by Hood and colleagues (Hood, 1978; Hood *et al.* 1978; Hood, Finkelstein & Buckingham, 1979). It was further developed by Geisler (1981, 1983), Finkelstein and Hood (1981), Hood and Greenstein (1982, 1990), Adelson (1982), Hayhoe, Benimoff and Hood (1987) and Walraven and Valeton (1984). The models in this framework are also able to account for related and more intricate phenomena of adaptations arising from more elaborate experiments than those described here. Reviews of this approach and the associated models can be found in Adelson (1982), Hood and Finkelstein (1986) and Hayhoe *et al.* (1987).

The class of models from this tradition is schematized in Fig. 2. Time is not explicitly included in these models and therefore one cannot use these models to compute responses to stimuli that are arbitrary functions of time. Some temporal effects are included in an *ad hoc* manner, however, and are crucial to the predictions of these models. (The fact that temporal effects are only partly included—that time is not an explicit parameter of the model—is why we refer to these as "static" models below.)

There are three component processes in these models: (i) a static nonlinear process (that is a nonlinearity that acts instantaneously and does not change over time); (ii) a multiplicative process that develops with time; and (iii) a subtractive process that develops with time. As implied by Fig. 2, the multiplicative and subtractive processes occur before the static nonlinearity and are assumed to be slow enough that they have no effect on the probe when it occurs at the onset of the background (SOA = 0).

Figure 3 further describes these three component processes by showing the response amplitude as a function of intensity for subcases containing various combinations of processes. The curve in Fig. 3(A) is the response function of the model in the dark and is determined only by the static nonlinear process (equivalently, therefore, it equals the response function for the static nonlinear process by itself in the dark). The static nonlinear function shown, and the one usually used, has the form

$$R(I) = \frac{I}{I+\sigma} \cdot R_{\max} \tag{1}$$

where I is the intensity of the light, σ the semisaturation constant, and $R_{\max}$ the maximum response of the system to that light.

Figure 3(B) considers the case where the static nonlinearity is the only process in the system. In this case, the incremental responses (ΔR) to incremental probes of intensity ΔI upon adapting fields of intensity A are given by

$$\Delta R(\Delta I) = R(\Delta I + A) - R(A). \tag{2}$$

Figure 3(B) shows the incremental responses to the probe as a function of the intensity of the probe ΔI when the probes are on a dark background [dashed curve—identical to that in Fig. 3(A)] or when they are on a background of intensity A' (solid curve). A' is the intensity that, when presented in the dark, produces the response shown by the dotted vertical line in Fig. 3(A). Since A' by itself produces a very large response, there is little response range left for the incremental probe stimuli so the maximal response to a probe on top of this background is much less than that in the dark. Indeed, the responses to all probes are reduced.

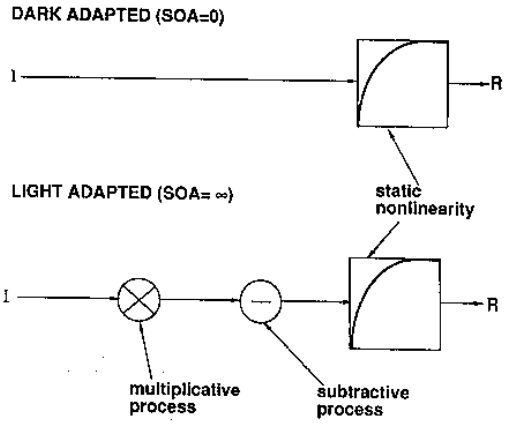

FIGURE 2. Schematic of static models of adaptation from the aperiodic tradition for the dark-adapted (SOA = 0, top) and the light-adapted state (SOA = ∞, bottom).

To fit the psychophysical data, a *constant-response or constant-ΔR assumption* is usually made. In particular, the test probe of intensity ΔI is assumed to be at threshold when the incremental response ΔR to the test equals a criterion amount, δ, as indicated by the dashed horizontal lines in Fig. 3. Thus, the value of ΔI at threshold is ΔI_0 where

$$\Delta R(\Delta I_0) = \delta. \tag{3}$$

When the static nonlinearity is the only process in the model, the incremental response is given by equation (2). Combining equations (2) and (3) gives

$$R(\Delta I_0 + A) - R(A) = \delta. \tag{4}$$

Following the dashed horizontal lines in Fig. 3(B) shows the effect for one value of the background field intensity, A'. Threshold, ΔI_0, is substantially elevated relative to

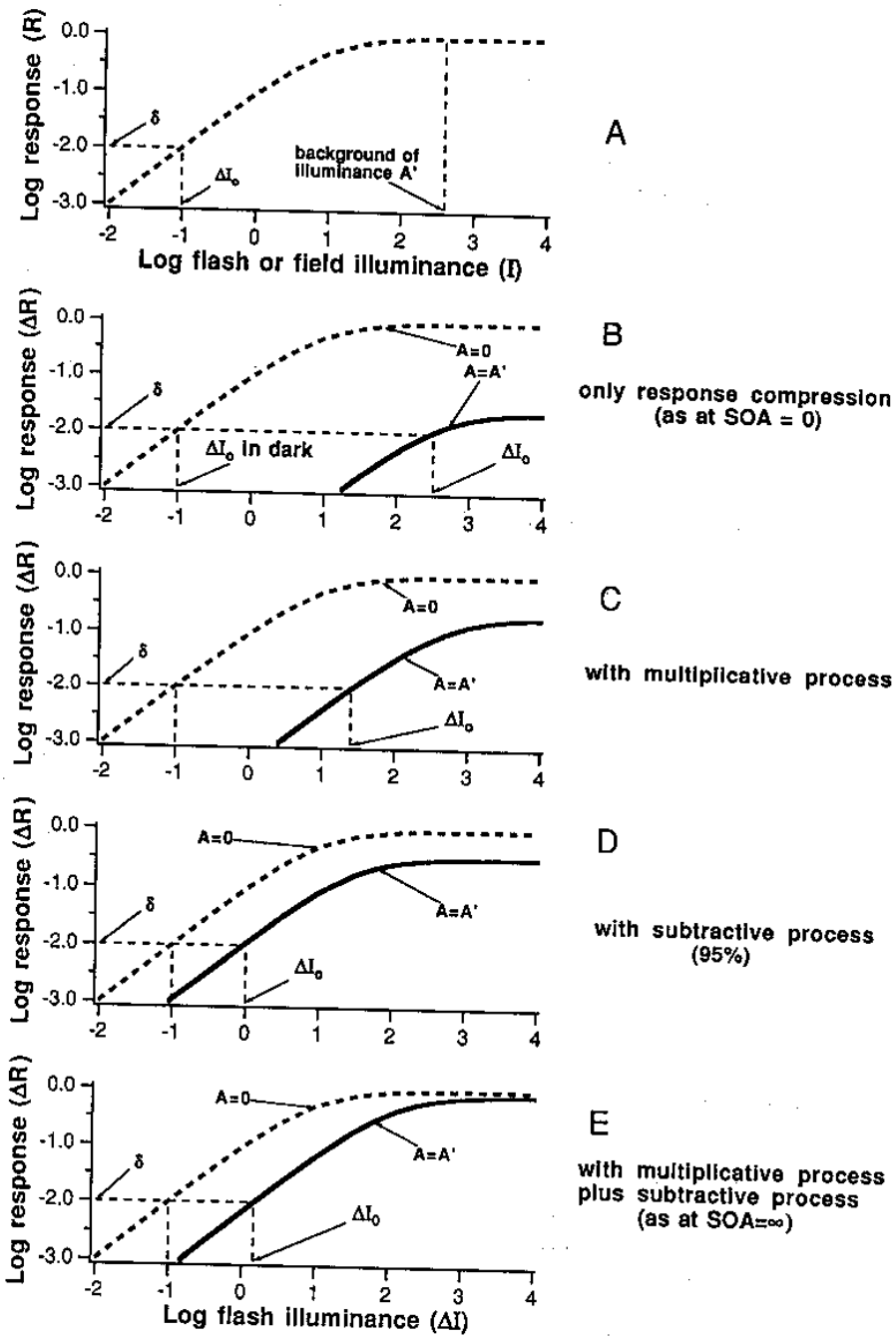

FIGURE 3. Illustration of the effects of the static nonlinearity, multiplicative process, and subtractive process in static models of adaptation from the aperiodic tradition. Log R is plotted on the vertical axis of (A) and log ΔR on the vertical axis of (B), (C) and (D). Log I is plotted on the horizontal axis of (A) and log ΔI on the horizontal axis of the (B), (C) and (D). Modified from Hood and Finkelstein (1986).

the threshold in the dark. Thus, when the static nonlinearity is the only process in the model the background light drastically reduces the response range and also the sensitivity to incremental lights. This effect was called "response compression" by Boynton and Whitten (1970).

At the onset of a background, the static models of Fig. 2 assume that only the static nonlinearity is effective, thus Fig. 3(B) describes the situation at the onset of background lights according to these models. Hence, the reduced range due to response compression exhibited in Fig. 3(B) is responsible for the large elevation in threshold at background onset that is predicted by these models. The smooth solid curve through the SOA = 0 condition data points in Fig. 1 is an example of such a prediction. [The psychophysical data for the SOA = 0 condition can be fitted by combining equations (1) and (4) and by estimating two parameters, σ and $\delta/R_{\max}$.]

The smooth dashed curve through the SOA = ∞ data in Fig. 1 shows the predictions of the class of static models of Fig. 2 for a steady background. To understand these predictions, however, both the multiplicative and subtractive processes have to be considered in addition to the static nonlinearity. The multiplicative and subtractive processes are assumed to come into play some time after the background has been turned on. Figure 3 illustrates the effects of these processes, singly [(C, D)] and together (E), on the function relating incremental response to incremental light intensity.

The solid curve in Fig. 3(C) shows the predicted response function for a multiplicative process in conjunction with the static nonlinearity. We mean by a multiplicative process one that decreases effectiveness of all lights by the same factor once the processs has come into play. In effect, this process multiplies the intensity of both background and probe lights by the same number $m(A)$, a number which is $\leqslant 1$ and which depends on the intensity A of the background light. The multiplication is assumed to be effective in the SOA = ∞ condition but not in the SOA = 0 condition of experiments like those in Fig. 1. In particular, the intensity ΔI of the probe becomes, in effect, $m(A)\Delta I$ and the intensity A of the background becomes $m(A)A$ where $m(A)$ is always between (or equal to) 0 and 1 and is equal to 1 in the dark or at SOA = 0. This class of adaptation mechanisms, called multiplicative by Adelson (1982), includes what others have called von Kries adaptation, cellular adaptation, automatic gain control, pigment depletion and dark glasses (see the reviews by Macleod, 1978; Shapley & Enroth-Cugell, 1984; Hood & Finkelstein, 1986). Figure 3 shows the effect on a background of intensity A' when $m(A') = 0.1$. Note that the addition of the multiplicative process means that the response function on a background of intensity A' [solid curve in Fig. 3(C)] recovers some of its response range and shifts to the left on the $\log \Delta I$ axis relative to the response function when only a static nonlinearity was present [solid curve in Fig. 3(B)]. The lower value of ΔI_0 for the solid curve in Fig. 3(C) relative to that for the solid curve in Fig. 3(B) is the result of two opposing influences of the multiplicative mechanism on threshold. The multiplicative mechanism decreases threshold by decreasing the effect of response compression, since the effective intensity of the background becomes $m(A')\cdot A'$. At the same time, it increases the value of threshold since the probe threshold has also become less effective, equaling $m(A')\cdot \Delta I$.

Figure 3(D) shows the subtractive process in conjunction with the static nonlinearity (and without a multiplicative process). A subtractive process decreases the effectiveness of prolonged lights (e.g. the background in the SOA = ∞ condition) by removing some of the signal. This process does not change the effectiveness of briefly presented lights (e.g. the probe in both conditions and the background in the SOA = 0 condition). The class of subtractive adaptation mechanisms includes what others have called discounting the background, subtractive adaptation, or high pass temporal filtering (e.g. Hurvich & Jameson, 1958; Jameson & Hurvich, 1972; Walraven, 1976; Shevell, 1978). When a subtractive process is present in conjunction with the static nonlinearity, the intensity A of the background becomes, in effect, $A - s$ where $s = 0$ in the dark (or at the onset of the background) and is always between (or equal to) 0 and A at other times; but the intensity ΔI of the probe is always unaffected since the probe is presented for only a short time. When subtraction is complete ($s = A$) and there is no multiplicative process, the response function on a background of intensity A at SOA = ∞ is identical to the response function on a dark background. Thus, relative to the function in Fig. 3(B) for the static nonlinearity by itself, this response function has recovered all of its range, and the threshold on this background will be unchanged from its dark-adapted value. Figure 3(D) shows the effect when the subtraction is incomplete. (In this case 95% of the background A' is removed via subtraction, that is, $s = 0.95\ A'$.) Notice that the response function at SOA = ∞ on a background of intensity A' [solid curve, Fig. 3(D)] is shifted down and to the right relative to the dark-adapted function (dotted curve) but it is not shifted as far as the response function for the static nonlinearity by itself [solid curve, Fig. 3(B)]. Thus, the system with incomplete subtraction recovers some, but not all, of the sensitivity it lost due to response compression [Fig. 3(B)].

In Fig. 3(E) both multiplicative and subtractive processes have been added to the static nonlinearity. The effective intensity A' of the background after it has been on for some time becomes $m(A')(A' - s)$ and the effective intensity ΔI of the probe is $m(A')\Delta I$. Notice in Fig. 3(E) that, although the value of ΔI for prolonged viewing (SOA = ∞) of background A' is above the value for ΔI_0 in the dark, it is substantially lower than the value of ΔI_0 at SOA = 0 [Fig. 3(B)]. The combined effect of the multiplicative and subtractive time-dependent processes is to decrease the value of ΔI_0 after background onset, although never decreasing it to the level in the dark. If subtraction is

complete, then the elevation in ΔL_0 at SOA = ∞ is due to the multiplicative effect on the probe intensity [e.g. $m(A')\Delta I$].

In short, static models of the class shown in Fig. 2 successfully predict the background-onset effect in the following way: threshold is greatly elevated at background onset by the response compression resulting from the static nonlinearity but, as the background stays on, multiplicative and subtractive adaptation processes pull the response to the background back down to a lower level leaving more response range for the response to the probe. Multiplicative and subtractive processes differ in that multiplicative, but not subtractive, also reduce the sensitivity of the system to the probe itself. If subtraction is complete, it is the multiplicative process that accounts for any threshold elevation in the SOA = ∞ (steady-state condition), e.g. for the Weber's-law-like behavior.

THE PERIODIC-STIMULUS TRADITION

The earliest use of periodic stimuli to study light adaptation was to measure at various mean illuminances the "critical fusion frequency"—the highest rate at which the observer could still see flicker when a rapid series of flashes was presented. It is now well known that this critical fusion frequency increases with increasing light levels although there is still some question about the exact form of this increase (see, e.g. Tyler & Hamer, 1990; Rovamo & Raninen, 1988, for some discussion and earlier references.) Subsequently, many studies measured contrast thresholds as a function of the frequency of sinusoidal modulation in either time or space (for reviews see, e.g. Graham, 1989; Shapley & Enroth-Cugell, 1984; Watson, 1986.) Our major interest here is in temporal vision, and the spatial case will be only briefly mentioned.

Figure 4 illustrates four ways of plotting the effects of mean illuminance on an observer's sensitivity to sinusoidal stimuli. The upper left panel shows a plot analogous to the plot of aperiodic results in Fig. 1. The amplitude threshold ΔI_0 is the difference between the peak illuminance and the mean illuminance or, equivalently for sinusoidal stimuli, equal to one-half the peak-minus-trough illuminance. The value of ΔI is plotted logarithmically on the vertical axis and I (the mean illuminance) logarithmically on the horizontal axis. Different curves give the results for different frequencies. As with aperiodic stimuli at SOA = ∞, amplitude threshold (ΔI_0) is first constant and then increases, at first slowly, and then more quickly until, prototypically, Weber's law is reached and ΔI_0 becomes approximately proportional to I, yielding a line of slope of 1 on log–log coordinates. (Thresholds for sinusoidal stimuli—either spatially or temporally-sinusoidal—are typically collected when the observer has been viewing the mean illuminance for some time, i.e. like the SOA = ∞ condition in Fig. 1.)

As indicated by the labels on the plots in Fig. 4(A), we will sometimes talk about these changes with mean illuminance as falling into *three regions*. At low mean

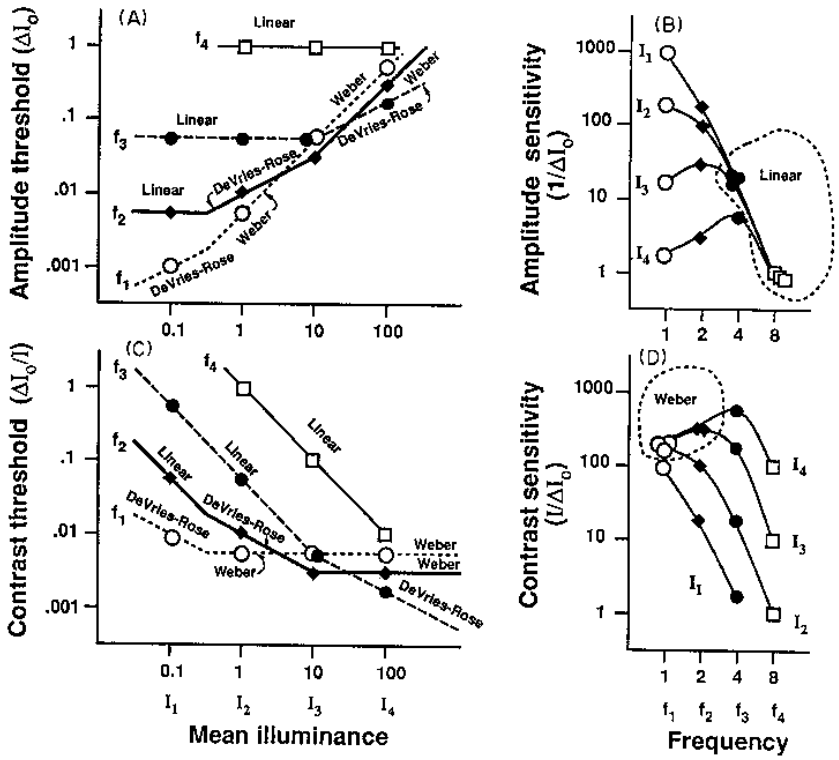

FIGURE 4. Four alternative ways of plotting visibility of sinusoidal stimuli that can vary in mean luminance and frequency. Modified from Graham (1989).

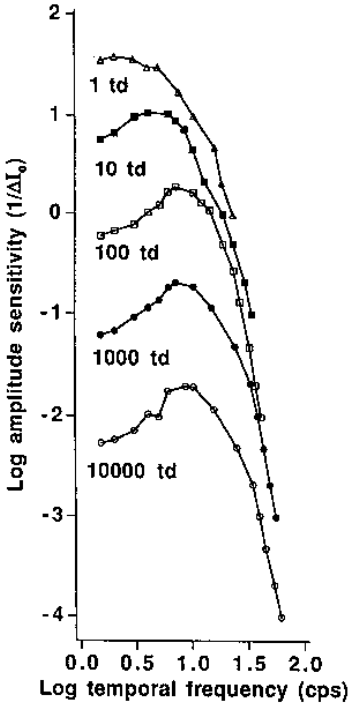

FIGURE 5. Sensitivity of a human observer to sinusoidal flicker. Amplitude sensitivity (vertical axis) is plotted as a function of the temporal frequency (horizontal axis) for different mean illuminances (different curves). Results from de Lange (1958).

illuminances, there may be a *linear* region where amplitude threshold ΔI_0 is constant [hence a horizontal line segment in Fig. 4(A)]. This kind of behavior is expected from a linear system as long as certain auxiliary assumptions are made, e.g. the constant-ΔR-assumption described above. At somewhat higher mean illuminances, there is a *de Vries–Rose* range (so-called because of theoretical considerations of quantal fluctuations associated with de Vries (1942) and Rose (1942, 1948) where amplitude threshold is increasing, as a square-root function of I [hence, a line segment with slope $+0.5$ in Fig. 4(A)]. Finally, there may be a *Weber* range at the highest mean illuminances where ΔI_0 increases approximately proportionally to I [hence a slope of approx. 1.0 in Fig. 4(A)]. A function for a particular stimulus may not contain all three regions, however, and pure examples of these regions usually exist for only a limited range of mean illuminances with smooth transitions in between. See, e.g. Kelly (1972) for examples.

The other panels of Fig. 4 show the same results as those in (A) but plotted in three different ways. The plot that we will find most useful here is shown in Fig. 4(B). The vertical axis shows the reciprocal of the amplitude threshold ($1/\Delta I_0$—usually called *amplitude sensitivity*) plotted logarithmically and the horizontal axis shows logarithmic frequency. Different curves now give the results for different mean illuminances. On this kind of plot the linear region (where ΔI_0 is independent of I) can be identified by the superposition of the curves for different mean illuminances [see points enclosed by dashed line in Fig. 4(B)]. Figure 5 shows an example of psychophysical results from de Lange's classic studies plotted in this manner (de Lange, 1952, 1954, 1958).

In the periodic-stimulus tradition, stimuli are often described in terms of their contrast, which is the amplitude divided by the mean illuminance, that is, $\Delta I/I$. Contrast varies between proportions of 0 and 1 for sinusoidal gratings, or, alternately, between percentages of 0 and 100%. (For other stimuli, however, notice that the analogous definition of contrast can go from zero to infinity.) Figure 4(C) shows contrast threshold $\Delta I_0/I$ plotted vs mean illuminance (both logarithmically) where different curves give the results for different frequencies. Here the linear region corresponds to a slope of -1, the de Vries–Rose region to a slope of -0.5, and the Weber region to a horizontal line segment.

Perhaps the most common plot in the periodic-tradition literature is that shown in Fig. 4(D). The vertical axis of this plot gives contrast sensitivity ($I/\Delta I_0$—the reciprocal of the contrast threshold) logarithmically—and the horizontal axis shows frequency logarithmically. The lowest measurable contrast sensitivity for a sinusoidal stimulus is 1.0 (corresponding to the maximal possible contrast of 1 or 100%). On this kind of plot the Weber region (where contrast threshold is independent of mean illuminance) is easily detected because the curves for different mean illuminances are superimposed [see points enclosed by dashed line in Fig. 4(D)].

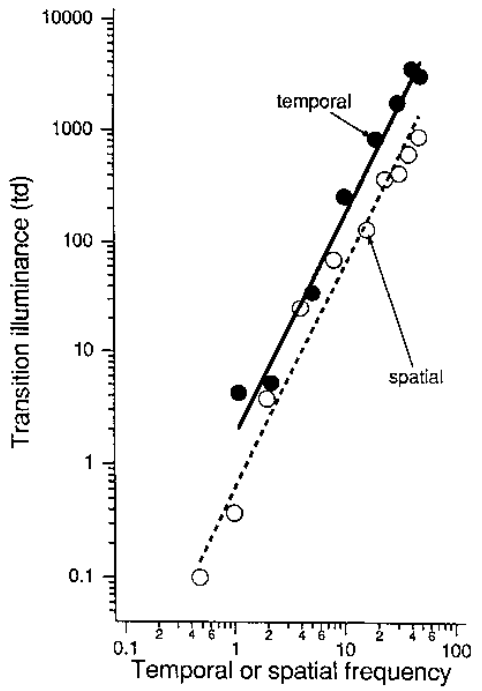

FIGURE 6. The relationship between spatial or temporal frequency (on horizontal axis) and the illuminance at which the transition from de Vries–Rose to Weber behavior occurs (on vertical axis). Points show experimental results. Straight lines have a slope of 2. Modified from van Nes *et al.* (1967).

How does this effect of mean illuminance interact with frequency? The typical effect is very similar for both spatial and temporal frequency and is illustrated in Figs 4 and 5. The interaction of mean illuminance and frequency can be described in terms of the illuminances at which the transitions between regions occur. In particular, the transition from linear to de Vries–Rose or that from de Vries–Rose to Weber behavior can be estimated for individual frequencies. It is well established that the higher the frequency, the higher the mean illuminances at which a given transition occurs. This can be seen in the left panel of Fig. 4 where curves are shown for four different frequencies, f_1 being the lowest and f_4 the highest. For both spatial and temporal frequency, van Nes, Koenderink, Nas and Bouman (1967) suggested a simple and elegant summary of the relationship between frequency (plotted on the horizontal axis of Fig. 6) and the mean illuminance at which the transition from the de Vries–Rose to the Weber region occurred (plotted on the vertical axis of Fig. 6). To a first approximation, the data are well represented by straight lines with a slope of 2 on log–log axes. That is, letting L_T be the illuminance at which the transition from de Vries–Rose to Weber behavior occurs and f be the frequency, then

$$L_T = \alpha f^2. \quad (5)$$

High-temporal-frequency linearity

The interaction between mean illuminance and frequency can be described in other ways. One can say, for example, that Weber behavior occurs at lower mean illuminances for low frequencies than for high. Notice that the curves in the contrast sensitivity vs frequency plot of Fig. 4(D) superimpose at the low-frequency end.

Or, of particular interest in this paper, one can point out that the curves in the amplitude sensitivity vs frequency plot [e.g. Fig. 4(B) and Fig. 5] tend to superimpose at the high-frequency end. Or, if not actually superimposing, they come much closer together at the high-frequency end so there is a clear high-frequency envelope. Superposition is more regularly found for temporal frequency than for spatial frequency, but even for spatial frequency, there is clear convergence. Many references can be found in Watson (1986) and Graham (1989). This behavior is often spoken of as high-frequency linearity, since superposition occurs whenever the amplitude threshold for a particular frequency stays constant over a range of mean illuminances, or, in other words, superposition occurs within the linear range for each frequency. Even though the linear range for each frequency may extend only over a small range of mean illuminances above threshold, the fact that both the linear and de Vries–Rose ranges shift with frequency means that there tends to be an overall high-frequency envelope to all the curves. We will refer to this phenomenon below as *high-temporal-frequency linearity* or the *high-temporal-frequency envelope.*

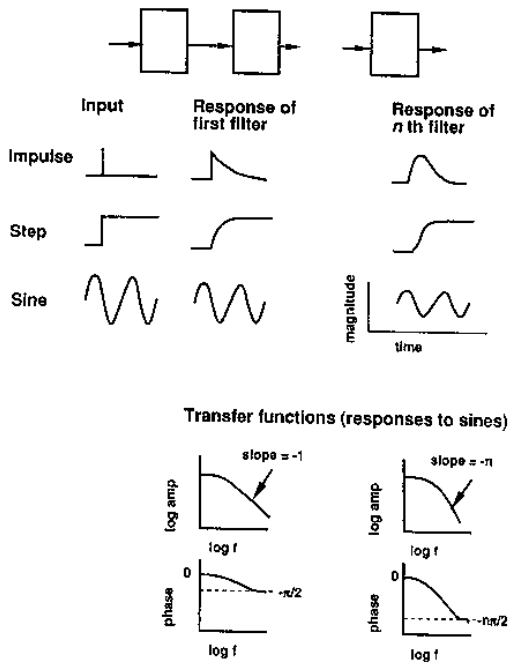

FIGURE 7. Responses to impulses, steps, and sinewaves by cascaded exponential filters.

Dynamic models of adaptation from periodic-stimulus tradition

Several models of light-adaptation dynamics have been proposed to explain the interaction between temporal frequency of periodic stimuli and intensity (Baylor, Hodgekin & Lamb, 1974; Dodge, Knight & Toyoda, 1968; Fuortes & Hodgekin, 1964; Kelly, 1961; Matin, 1968; Sperling & /Sondhi, 1968; Sperling, 1989; Tranchina, Gordon & Shapley, 1984; Tranchina & Peskin, 1988). We will look at one of these models in some detail, showing its predictions of high-temporal-frequency linearity, and then attempt to give some insight into why such a prediction is made.

Sperling and Sondhi's model. We explore the model of Sperling and Sondhi (1968) in detail because: it is a model that is computable for arbitrary temporal stimuli; its substages appear in both physiological and psychophysical models; and, as the original investigators showed, it does quite well at accounting for many aspects of psychophysical detection thresholds, including sensitivity as a function of temporal frequency at different mean illuminances.

A basic component of Sperling and Sondhi's temporal model, and one that appears in many other models as well, is a low-pass filter of the sort sometimes called an RC stage, or a leaky integrator, or an exponential filter. Figure 7 top shows n of these exponential filters connected so that the input of one is the output of the one before it. (The Appendix contains equations describing these filters.) Underneath the sketch of the filters are shown the responses out of the first and nth filters to several stimuli (impulse, step, and sine—sketched at the left in different rows). The responses of one filter by itself (see middle column labeled "Response of first filter") to

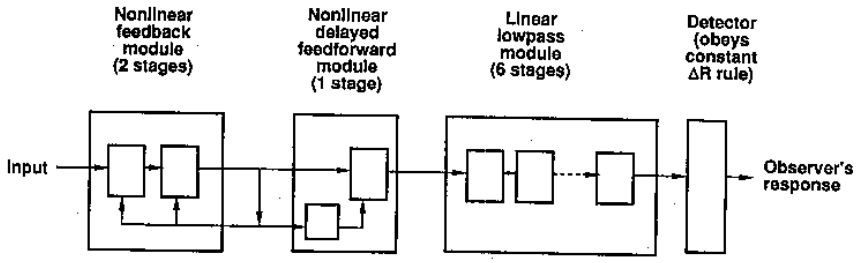

FIGURE 8. Diagram of Sperling and Sondhi's (1968) model of the dynamics of light adaptation, a model from the periodic tradition.

an impulse of light has an abrupt onset followed by an exponential decay to baseline (the time-constant of the decay is a parameter describing the filter). The response of a cascade of n such filters to an impulse has a less abrupt onset and a somewhat different shaped decay (mathematically, it is described by a gamma function). The response of one filter to a step gradually increases to some asymptote as does the response of the cascade of n such filters (but with somewhat different shapes). The response to a sine-wave is, as for all linear time-invariant systems, a sine-wave, but the amplitude of the response will depend on the frequency as well as the amplitude of the sine-wave stimulus. This dependence is shown in the second row from the bottom of the figure by the transfer functions that give the amplitude of the sinusoidal response as a function of the frequency of the stimulus sine-wave (where the amplitude of the sine-wave stimulus is held constant). Notice that either the single exponential filter or the cascade of n filters responds well to all low temporal frequencies but begins to respond much less well as the frequency gets higher. The slope of the high-frequency decline on these log–log plots equals $-n$. The very bottom row sketches the phase of the response.

The exponential filters just described are linear systems. Sperling and Sondhi's model is composed of such filters with one very important added nonlinearity. Following Fuortes and Hodgekin (1964) and others, Sperling and Sondhi postulated that the time-constants of some of the exponential filters would be shortened (and their gain would be decreased) by feedback or feedforward signals. Their full model is diagrammed in Fig. 8. It contains four modules. Difference equations describing the first three of these modules are contained in the Appendix. (1) The first module is a feedback module that consists of two stages of exponential filtering. The input to this module is the stimulus itself. The output of the module feeds back into the module to shorten the time constants of each of the individual filters. (2) The second module, whose input is the output from the feedback module, is a feedforward module which contains one stage of exponential filtering. The time constant of this filter is modified by a control signal, which is a filtered version of the input to the module. (3) The third module is a pure low-pass module consisting of six stages of exponential filtering. (4) The fourth module is a detector stage that produces a "yes" or "no" from the observer depending on whether the output from the previous modules was above or below a criterion; the behavior of this detector stage is consistent with the constant-response assumption of equation (3)

$$\text{if} \quad \max_t \Delta R(t) > \delta \quad \text{then observer says "yes"}$$
$$\leqslant \delta \quad \text{then observer says "no"} \qquad (6)$$

or, equivalently, at threshold

$$\max_t \Delta R(t) = \delta. \qquad (7)$$

Several properties of this model are worth making explicit. First, it assumes only a single channel (see

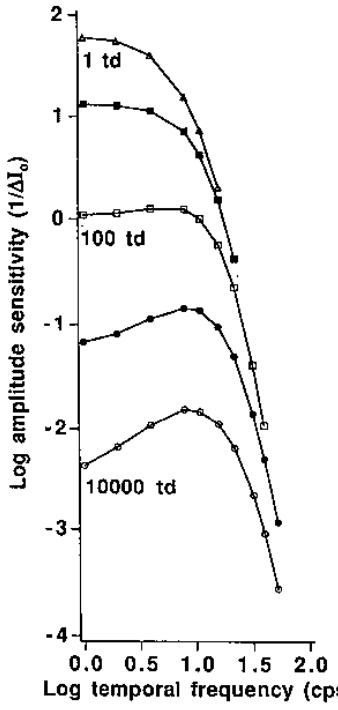

FIGURE 9. Predictions of Sperling and Sondhi's model for detection of sinusoidal flicker. Amplitude sensitivity (vertical axis) is plotted as a function of temporal frequency (horizontal axis) at different mean illuminances (different curves). The parameter values were similar to those used by Sperling and Sondhi (1968) and were as follows: in the feedback module, the time constant for each of the two exponential filters was 25 msec (in the dark). In the feedforward module, the time constant of the filter on the straight-through path was also 25 msec (in the dark) and that of the filter delaying the control signal was 15 msec. In the low-pass module the time constant of each of the six exponential filters was 6 msec. The criterion ΔR used for the predictions in this figure was 0.002.

comments in the Introduction). Second, there is no "noise," i.e. no source of variability from trial to trial (see Discussion). Third, there is no static nonlinearity (although the feedback and feedforward modules introduce some nonlinearity between the response to a probe and the probe intensity).

Predictions from Sperling and Sondhi's model. Sperling and Sondhi (1968) compared the predictions of their model to several sets of psychophysical results, including sensitivity as a function of the temporal frequency and the mean intensity of flickering stimuli. In particular, they compared their model's predictions to de Lange's flicker data, some of which is shown in Fig. 5. Figure 9 shows our recalculation of their predictions for the temporal-flicker data (using parameters in the same range they used) displayed as amplitude sensitivity vs flicker frequency. The fit between model predictions and empirical results was rather good although there were some problems, particularly at low frequencies, as pointed out by the authors. For our purposes here, the most important point is that the predicted functions of amplitude sensitivity vs temporal frequency share a common high-frequency envelope.

Sperling and Sondhi (1968) also compared the models' predictions to several sets of thresholds from the aperiodic-stimulus literature (in particular, thresholds on a steady background as a function of duration of the probe). The model did quite well. But they did not attempt to predict the background-onset effect.

Why high-frequency linearity. The general idea behind how this kind of model produces the high temporal-frequency envelope is as follows. For high temporal frequencies, two different effects of light adaptation balance each other; in particular, the shortening of the time constants compensates for the reduction of gain

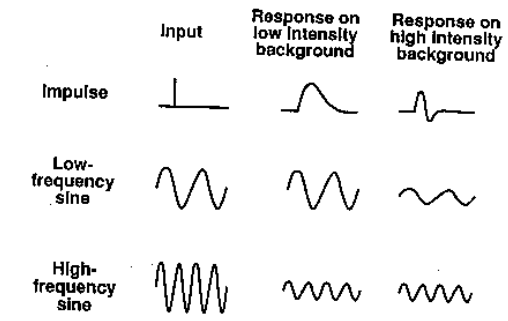

FIGURE 10. Responses to impulses and sine-waves on backgrounds of low intensity (middle column) or high intensity (right column) as predicted by typical models from the periodic tradition.

(of area under the impulse–response). This effect is visible in Fig. 10, which sketches the responses to three stimuli in the left column (impulse, low-frequency sine, and high-frequency sine) on a low-intensity background (middle column) and again on a high-intensity background (right column). In models like Sperling and Sondhi's, increasing the adapting intensity shortens the time–course of the impulse–response (perhaps even causing a monophasic impulse–response to become biphasic). In such models, this shortening of time–course is accompanied by a decrease in the area underneath the impulse–response. (This decrease occurs even when the height of the impulse–response is relatively unaffected as in the example of Fig. 10—compare the top middle to the top right response. In fact, the height may also be decreased for a further decrease in area underneath the impulse–response.) Thus there will be less gain at high light levels than at low (each photon will have less effect since the area under the impulse–response is smaller),

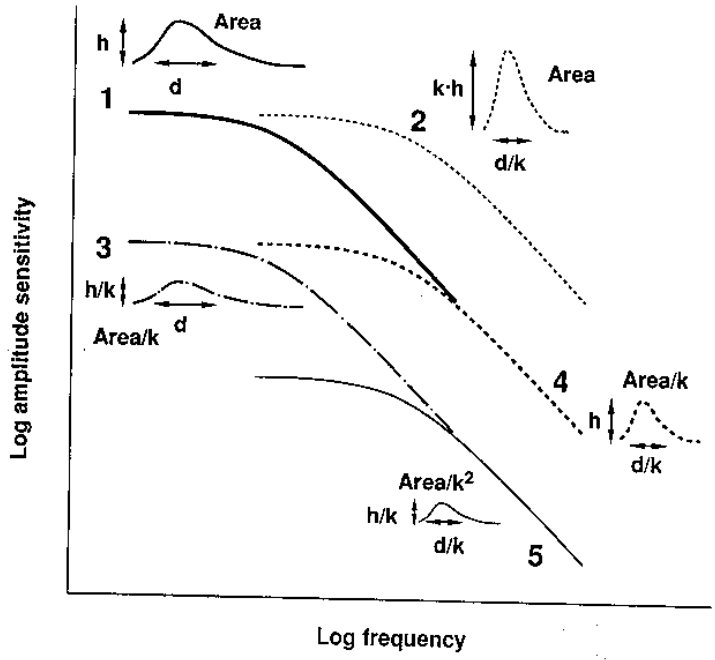

FIGURE 11. Effects of changing area, height, and duration of impulse–response on transfer function.

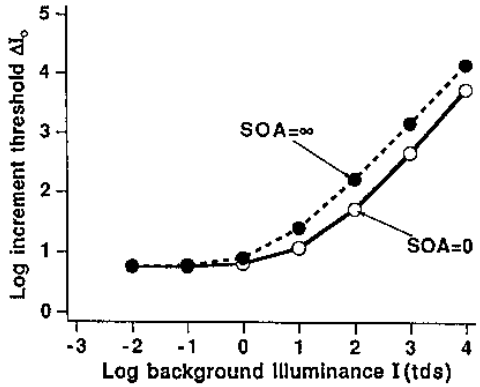

FIGURE 12. Predictions of Sperling and Sondhi's model for an aperiodic test stimulus superimposed on an aperiodic background stimulus when the test comes on at the same time as the background (SOA = 0) or at a much later time (SOA = ∞). Parameter values are as in Fig. 9 except that criterion ΔR was 0.05. (Using other values for criterion ΔR did not produce a bigger background-onset effect.)

but there will be increased temporal resolution (the duration of pulse–response is shorter). For lower temporal frequencies, the decreased gain (decreased area under the impulse–response) at high illuminances means a decreased amplitude of response at high illuminances. (Note that the middle-row, right-hand response is smaller than the middle-row, middle-column response.) For high temporal frequencies, however, the increased temporal resolution can compensate for the decreased gain so that the amplitude of the response can remain the same at quite different intensities as if the system were linear. (Note that the lower middle and lower right responses have the same amplitude.)

Graphs of the impulse–responses at many different background intensities are given in Fig. 7 of Sperling and Sondhi (1968) for parameters very similar to the ones we used for Fig. 9 here. The width at half-height of the initial excitatory phase of the impulse–response is about 100 msec long on a 7×10^{-3} td background and about 15 msec on a 7×10^{6} td background.

An alternative illustration in terms of transfer functions. (This paragraph can be skipped without loss of continuity.) In Fig. 11, log sensitivity is plotted as a function of log frequency. First, consider the effect of a pure time–course reduction with no change in gain, that is, the effect of reducing the duration of the impulse–response while keeping the area underneath it—the total effect of each photon—constant (implying an increase in the height of the impulse–response). This simply shifts the function horizontally on log–log coordinates rightward toward higher temporal frequencies as in the shift from curve 1 to curve 2 in Fig. 11. On the other hand, a pure gain change with no time-constant change, that is, a reduction in the area of the impulse–response while keeping its duration constant (which implies a reduction in height), moves the function straight down as in the shift from curve 1 to curve 3 in Fig. 11. Models like Sperling and Sondhi's assume both a time-constant reduction and a gain change, that is, a decrease in both the duration and the area of the impulse–response. If the decrease is exactly the same for both (so that height of the impulse–response remains exactly constant), then the transfer function moves over and down by equal amounts (as in the shift from curve 1 to curve 4 in Fig. 11). If the area underneath the impulse response decreases even faster than the duration (as it does in many models), the curve moves down more than it moves over (see curve 5). Whether such movement produces a common high-temporal-frequency envelope (and therefore the phenomenon we called high-temporal-frequency linearity) between the function at a low mean illuminance (e.g. curve 1) and that a higher mean illuminance (e.g. curve 4 or 5) depends both on the exact relationship between gain and time–course changes as well as on the steepness of the high-frequency decline in both curves.

COMPARING ONE TRADITION'S MODELS WITH THE OTHER TRADITION'S RESULTS

As expected, a typical static model from the aperiodic-stimulus tradition does predict the background-onset effect and a typical model from the periodic-stimulus tradition does predict the high-temporal-frequency linearity. Now we ask whether models from one tradition can predict the phenomena from the other tradition, phenomena against which they have never been tested. They cannot, as is particularly clear in the case of the two phenomena we are focussing on here.

The periodic-tradition models and the background-onset effect

As shown in Fig. 1, the psychophysical threshold for a probe is highest when it is coincident with the onset of

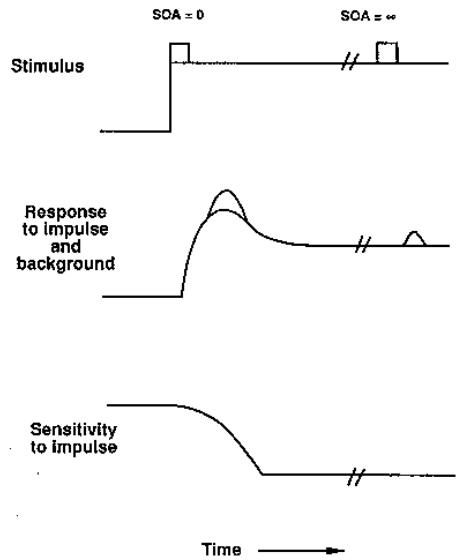

FIGURE 13. The periodic-tradition model's response to test stimuli coincident with the onset of the background (SOA = 0) or at a much later time (SOA = ∞). The stimuli are sketched in the top row, the responses of the model in the middle row, and the underlying sensitivity of the model (the reciprocal of the test intensity necessary to produce a criterion amplitude of response) in the bottom row.

the background and then decreases for longer SOAs. Further, the log ΔI vs log I curve rises much more steeply when the increment is coincident with onset than when it occurs on a steady background.

As Fig. 12 shows, the Sperling and Sondhi model does not predict this background-onset effect. Instead, it predicts that the thresholds for probes coincident with the onset of the background are lower, not higher, than the threshold for probes that come later. Further, both predicted curves rise in approximate proportion to the background illuminance I, but in psychophysical results ΔI at onset is approximately proportional to I^2 and ΔI in the steady state is approximately proportional to I. In retrospect, it is easy to understand why models like Sperling and Sondhi's do not predict the background-onset effect. As sketched in Fig. 13 bottom row, this model predicts that sensitivity to an impulse decreases monotonically with time after step onset. (Indeed, it is this reduction in sensitivity that catches up with the system's response to a step and causes it to come down to produce the transient in the step response at high mean luminances shown in the middle row.) This monotonic decrease in sensitivity after onset means that a response to an increment of constant ΔI is greatest at step onset and monotonically decreases thereafter as shown by the sketched impulse–responses in the middle row of Fig. 13.

The aperiodic-tradition models and high-temporal-frequency linearity

Making the aperiodic static model dynamic in time—MUSNOL. To ask whether the class of models from the aperiodic tradition can predict high-frequency linearity requires specifying these models in time at least to the extent necessary to predict their responses to sinusoidally-varying stimuli. We know of only one model in this aperiodic tradition that adds time as an explicit variable. For the dark-adapted case, Geisler (1981) added two low-pass filters as shown in Fig. 14 by the little boxes labeled LP (for "low pass"). His low-pass filters were one-stage exponential filters but more generally they might be cascades of exponential filters. The first filter LP_1 largely sets the time–course of the response as it has a time constant considerably longer than the second filter.

This final low-pass filter LP_D might be thought of either as more temporal filtering occurring at a relatively low level in the visual system or as an integrator in the decision mechanism designed to prevent detection of very brief responses. Without this filter, detection occurs for very brief responses to the probe at earlier and earlier times on the leading edge of the step responses. Without the LP_D, these very brief responses are detected by the observer. Then the background-onset effect is not predicted to occur because these brief responses are occurring before the response to the background is large enough to produce response compression. But, these responses are very brief and the small amount of temporal integration produced by LP_D makes them undetectable. (See Geisler, 1979, p. 175, for discussion.)

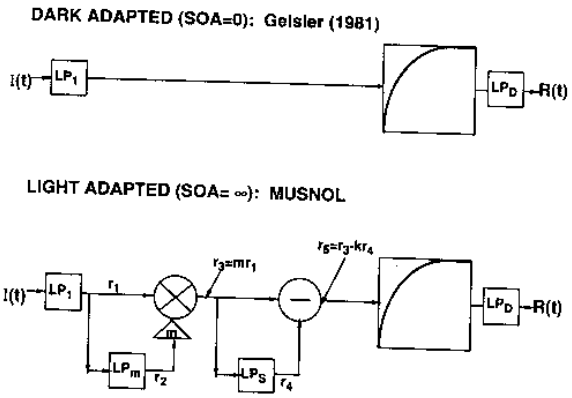

FIGURE 14. Diagram of MUSNOL (for multiplication-subtraction-nonlinearity), the dynamic version of the aperiodic-tradition model illustrated in Fig. 2. The boxes marked LP here are low-pass modules containing 1 or more exponential stages.

In the following, we will sometimes refer to the final low-pass filter as the Geisler fix.

Geisler's dynamic version of the aperiodic-tradition model was only designed to account for brief aperiodic stimuli in the dark. Thus, Geisler did not make the time-dependent multiplicative and subtractive adaptation processes computational in time. With help from Mary Hayhoe and in accord with a suggestion from Adelson (1982), we attempted to make the full model shown in Fig. 2 explicit in time. Instead of just assuming that the multiplicative and subtractive processes were ineffective at SOA = 0 and fully effective in the steady state (SOA = ∞), we now explicitly added temporal filters in the multiplicative and subtractive processes as shown in Fig. 14. These temporal filters, called LP_m and LP_s for the multiplicative and subtractive processes respectively, were assumed to be cascades of exponential filters (in general, more complicated filters could be considered). The signal $r_1(t)$ leaving the first low-pass filter stage (LP_1) is multiplied by $m(t)$ which is a nonlinear transformation of $r_2(t)$, a slowed-down version of $r_1(t)$. Specifically, as indicated on the diagram, $r_2(t)$ is the output of the low-pass filter LP_m in the multiplicative loop and, at each point in time, the value of $m(t)$ depends nonlinearly on $r_2(t)$. In particular,

$$m(t) = C/[C + r_2(t)] \tag{8}$$

where C is a constant. The signal $r_3(t) = m(t) \cdot r_1(t)$ leaving the multiplicative stage is then reduced in size by the signal $kr_4(t)$, which is subtracted point by point in time from $r_3(t)$ to produce $r_5(t)$. The signal $kr_4(t)$ is produced by low-pass filtering $r_3(t)$ by the filter LP_s. The filter's output is normalized such that when $k = 1.0$ the steady-state response $kr_4(\infty)$ out of LP_s is the same as the steady-state response $r_3(\infty)$ and complete subtraction occurs [i.e. $r_5(\infty) = 0$]. Next the signal $r_5(t)$ goes through the static nonlinearity. The final low-pass filter LP_D is the same as in the upper panel of Fig. 14. Detection of the test probe occurs when the peak of the response exceeds a fixed criterion.

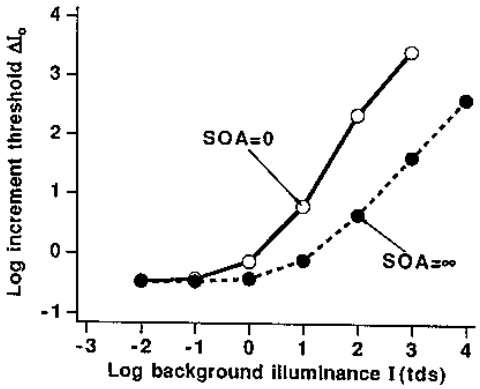

FIGURE 15. Predictions of MUSNOL for an aperiodic test stimulus superimposed on an aperiodic background stimulus when the test comes on at the same time as the background (SOA = 0) or at a much later time (SOA = ∞). Parameter values are as follows. The low-pass filter labeled LP_1, had 1 exponential stage with a time constant of 300 msec. That labeled LP_M had 5 exponential stages each at 8 msec. LP_S had 5 stages each at 15 msec. And LP_D had 1 stage with a time constant of 20 msec. The constant C of the multiplicative function $m(t)$ in equation (8) was 10. The subtractive constant k was 1.0. The static nonlinearity had the form of equation (1) with a semisaturation constant σ of 0.1625 and $R_{max} = 1.0$. The criterion ΔR was 0.05.

This dynamic version of the static model from the aperiodic-stimulus tradition will be called "MUSNOL" for multiplicative, subtractive, nonlinear model.

MUSNOL and the background-onset effect. Figure 15 shows some successful predictions from MUSNOL for the background-onset paradigm. It turned out to be a good deal harder to make MUSNOL predict the background-onset effect that we had anticipated. After the model is made dynamic with the multiplicative and subtractive processes developing over time, it is still nontrivial to arrange the parameters so that the threshold is elevated sufficiently at SOA = 0. For one thing, as mentioned earlier, the final low-pass filter (the Geisler fix) is crucial to prevent detection of very brief responses occurring at background onset. To simulate this model, we used Geisler's values for LP_1 and LP_D and specified the parameters of the other components. The legend of Fig. 15 contains the values of these parameters. The value of the constant k in the subtractive stage was set so that in the steady state r_3 equaled $k \cdot r_4$ and the signal attributed to the background was completely removed. This is referred to in the literature as complete subtraction or completely discounting the background. The value of C in equation (8) was estimated from the SOA = ∞ data in Fig. 1. Since the background signal was completely removed, the only factor increasing threshold for prolonged backgrounds is the multiplicative mechanism. Therefore, the SOA = ∞ data in Fig. 1 provide an estimate of the value $m(\infty)$ in equation (8). The number of stages and time constants of LP_m and LP_s were set so that the multiplicative process was fast relative to the subtractive process.

As shown in Fig. 15, MUSNOL captures the two key aspects of the background-onset effect. First, the threshold is always higher at the onset of a background. Second, the slopes of the high intensity limbs are approximately correct; for the SOA = ∞ curve, the slope is 1.0 and it is substantially steeper than 1.0 for the SOA = 0 curve.

MUSNOL does not predict high-temporal-frequency linearity. Figure 16 shows the predictions of MUSNOL for amplitude sensitivity as a function of the temporal frequency and mean illuminance of flickering stimuli. A comparison with the data in Fig. 15 reveals that MUSNOL completely fails to capture the high-frequency-linearity effect. The curves for different mean illuminances do not share a common high-frequency envelope. Indeed, they do not even begin to converge—they remain exactly parallel to one another out to the highest frequencies measurable. Further, the slope of the high-frequency decline is too shallow, although this problem is easily fixed by adding more stages in the final low-pass filter.

The reason MUSNOL fails to predict high-temporal-frequency linearity is somewhat difficult to see. First notice that high-temporal-frequency linearity (or a common high-frequency envelope) requires that thresholds for different temporal frequencies be affected differently by changes in mean level; in particular, the amplitude thresholds for the very high temporal frequencies should remain constant over a range of mean luminances while those for lower temporal frequencies are increasing. In MUSNOL, only the static nonlinearity and the multiplicative process are capable of producing changes in amplitude threshold with changes in mean illuminance. (The other components of the model, including

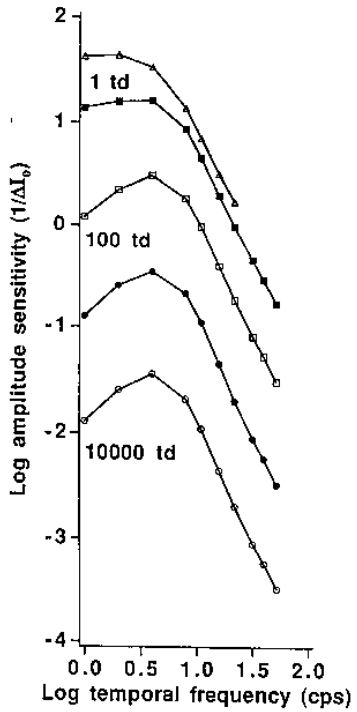

FIGURE 16. Predictions of MUSNOL for detection of sinusoidal flicker. Amplitude sensitivity (vertical axis) is plotted as a function of temporal frequency (horizontal axis) at different mean luminances (different curves). The parameter values are as in Fig. 15.

the subtractive mechanism, are linear systems.) But, the static nonlinearity is frequency-independent and the multiplicative process's effect is largely frequency-independent, being primarily determined by the recent time-averaged luminance. [Although the value of $m(t)$ will fluctuate somewhat when the stimulus is flickering at a very low temporal frequency, when the stimulus is flickering at a high temporal frequency the value of $m(t)$ will be effectively constant across time and dependent only on the mean illuminance. Thus the multiplicative process's effect will be the same for all but the lowest temporal frequencies.]

An alternative way to express the failure of MUSNOL to predict linearity at high temporal frequencies is in terms of the changes in the impulse–response of the system with increases in mean luminance as seen schematically in Figs 10 and 11. In MUSNOL, at high mean luminances there is no decrease in the duration of the impulse–response to compensate for the decrease in area of the impulse–response caused by the multiplicative process. That is, the multiplicative process reduces the height of the impulse–response but there is no offsetting change in its shape that is dependent upon mean level.

MERGING THE TWO TRADITIONS' MODELS

The MUSNOL model (based on the static models from the aperiodic tradition) can predict the background-onset effect (from the aperiodic-stimulus tradition) but cannot predict the high-temporal-frequency linearity (from the periodic-stimulus tradition). The Sperling and Sondhi model (from the periodic-stimulus tradition) can predict the high-temporal-frequency linearity (from the periodic-stimulus tradition) but cannot predict the background-onset effect (from the aperiodic-stimulus tradition).

One would like to merge the models from these two traditions in a way that retains the successes of each while eliminating the failures. There are various ways to merge the models that do not accomplish this aim; we discuss several below. There are also ways of merging them that do accomplish this aim; we present two below. In order to conveniently mention a number of auxiliary points, we present the first successful merged model by starting from the model of the aperiodic tradition and modifying it. We then present the second by starting from the model of the periodic tradition and modifying it. In fact, however, as will become clear, these successful merged models have more in common than the initial presentation might suggest.

Starting with the aperiodic-tradition model

Remember that MUSNOL fails to predict high-frequency linearity because the multiplier turns down the responses to all frequencies of stimulation equally, including the high temporal frequencies, thus producing Weber's law at all frequencies at high enough mean luminances. This way of explaining MUSNOL's failure suggests making the multiplicative process explicitly frequency-dependent so that it affects only the lower temporal frequencies of stimuli (where one wishes to obtain Weber's law at high mean luminances) without affecting higher temporal frequencies of stimuli.

Making multiplicative process frequency-dependent fails. One might think that, to accomplish this, the filter in the multiplication loop in MUSNOL should be made band pass instead of high pass so that it would respond neither to the mean luminance nor to the high-frequency flicker in a high-frequency flickering stimulus [$r_1'(t) = 0$ and thus $m(t) = 1.0$ for such stimuli]. But then the multiplicative process would also not respond to a brief probe on a steady background and thus could not correctly predict Weber's law for such probe stimuli.

Replacing the front end with a frequency-dependent gain-changing process succeeds. Many models from the periodic tradition, in particular, Sperling and Sondhi's model discussed above, exhibit high-frequency linearity because, as mean luminance increases, temporal resolution increases in a way that compensates for the decreasing overall gain (i.e. the area under the impulse–response or the amplitude sensitivity at d.c.). Thus the degree to which mean luminance changes amplitude threshold is highly dependent on temporal frequency. It is exactly this property that the MUSNOL multiplicative process lacks since the MUSNOL process changes gain uniformly for all frequencies but the very lowest. This observation suggests that replacing the multiplicative process in MUSNOL with a frequency-dependent gain-changing process from the periodic-tradition would work. A particularly simple process with the desired frequency-dependence is a feedback module like that in the Sperling and Sondhi model—that is, a cascade of exponential filters with feedback from the output of the last filter to each of earlier filters. Similar feedback schemes occur in other models (e.g. Matin, 1968). Since a feedback module incorporates low-pass filtering, we used it to replace both the first low-pass filter and the multiplicative process of MUSNOL. (Allowing the time-constant of the initial filters to change has been mentioned previously as one way of changing the gain for an aperiodic test stimulus; see Geisler, 1981, p. 430 for example. Here such a change is incorporated in a computable process.) This replacement produces the model sketched in Fig. 17(A), which has a feedback module followed by the subtraction, static nonlinearity, and final low-pass filter of MUSNOL. We used four stages of feedback in the feedback module as a compromise between two other desired features. The fewer the stages the smoother and less complicated the step and probe responses produced by the module. But the greater the number of stages the closer one can get to Weber's law at low temporal frequencies or for probes on steady backgrounds (see, e.g. Sperling & Sondhi, 1968, p. 1135). We used six stages in the final low-pass filter in order to produce a more realistic high-frequency slope. The other parameters of the model were chosen to produce reasonably successful predictions of both phenomena and are given in the figure legend.

As can be seen in Fig. 17(B), the amplitude-sensitivity vs frequency curves predicted by this model are much

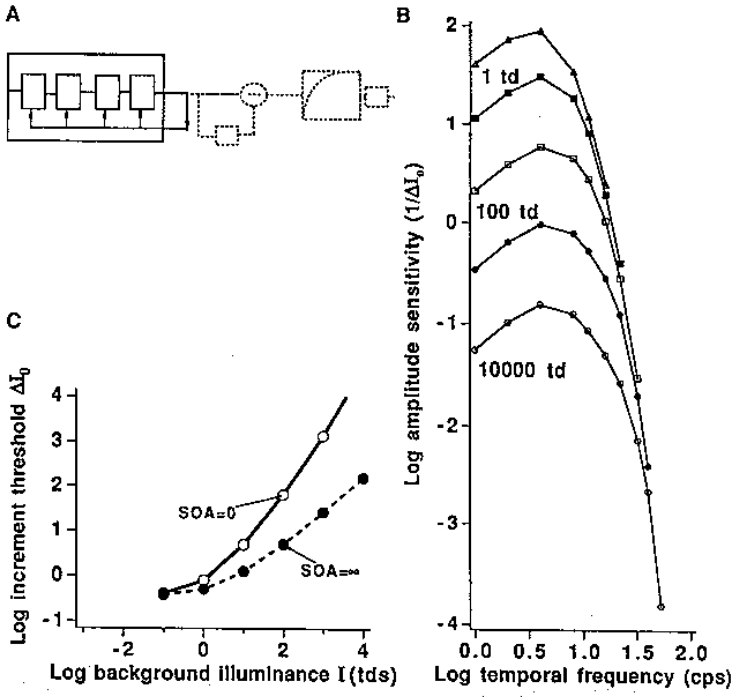

FIGURE 17. (A) Shows a sketch of the first merged model where a feedback module is followed by subtraction, a static nonlinearity, and a final low-pass filter. (B) Shows its predictions for sinusoidal flicker. (C) Shows its predictions for an aperiodic test stimulus superimposed on an aperiodic background stimulus. Parameters values for this model are as follows. In the feedback module there were 4 stages of exponential filters each with a time constant (in the dark) of 20 msec. The subtraction was identical to that in MUSNOL (i.e. the subtractive constant k was 1.0 and the low-pass filter had 5 exponential stages each with a time constant of 15 msec). The static nonlinearity had the form of equation (1) with a semisaturation constant σ of 0.065 and $R_{max} = 1.0$. The final low-pass filter was identical to that used in the Sperling and Sondhi model predictions (i.e. it had 6 stages each with a time constant of 6 msec). The criterion ΔR was 0.02 for the periodic stimuli (B) and 0.05 for the aperiodic stimuli (C).

closer together at the high-frequency end than at the low-frequency end. In other words, unlike the predictions of MUSNOL, they show high-frequency linearity. Further, as can be seen in Fig. 17(C), this merged model does predict the background onset effect. Thus, qualitatively at least, this merged model can predict the phenomena from both traditions.

Starting with the periodic-tradition model

The Sperling and Sondhi model from the periodic tradition (and also the feedback module by itself) fails to predict the background-onset effect. What is needed for the background-onset effect? Based on the preceding discussion, the response that goes into the static nonlinearity needs to be much larger at the onset of the background than later. If it is, the response to the probe at SOA = 0, which occurs simultaneously with response to the onset of the background, will be more compressed than the response to the probe at SOA = ∞, which occurs after the response to the background has reached its steady state.

Adding only a static nonlinearity fails. The step responses out of the Sperling and Sondhi model do have a transient component at high mean luminances. But there is no static nonlinearity after these responses (although both the peak and the steady-state responses are compressive nonlinear functions of intensity). Thus it seemed worthwhile to try a static nonlinearity inserted in the Sperling and Sondhi model to see if this modification would allow the model to successfully predict the background-onset effect. We tried the same function used in MUSNOL [see equation (1)] with several different values of the semi-saturation constant. We also tried the static nonlinearity in two different places, before and after the final low-pass filter. There was never any hint of a background-onset effect. The reason seems to be that the peak/steady-state ratio in the step responses of Sperling and Sondhi's model is never very large (<2 when the background intensity is high enough to have elevated threshold on a steady background by 3 log units above the dark-adapted value and no transient component at all when the background intensity is high enough to have elevated threshold by 1.5 log units). This does not leave much room within which the static nonlinearity can have an effect. (By contrast, in the MUSNOL calculations we did, the subtraction was complete so the steady-state response was zero. Thus the peak/steady-state ratio is infinite in our calculations.) Although we tried only static nonlinearities of the form of equation (1), it seems unlikely that any static nonlinearity inserted into the Sperling and Sondhi model could produce the background-onset effect.

Adding subtraction plus a static nonlinearity succeeds. We next tried adding both the subtractive process and

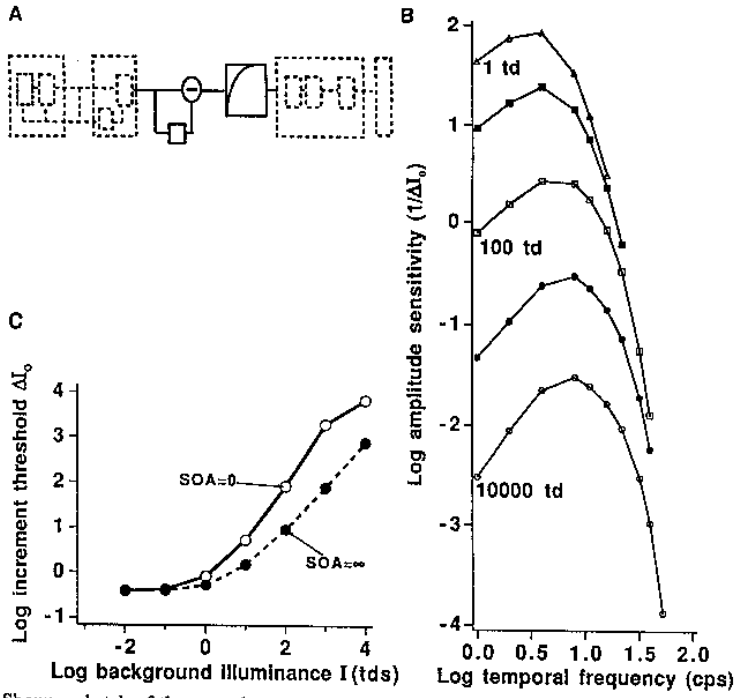

FIGURE 18. (A) Shows a sketch of the second merged model where subtraction and a static nonlinearity was inserted into the model of Sperling and Sondhi (1968) before the final low-pass filter. (B) Shows its predictions for sinusoidal flicker. (C) Shows its predictions for an aperiodic test stimulus superimposed on an aperiodic background stimulus. The parameters for the feedback and feedforward modules (found at the front end of this model) and for the final low-pass filter are identical to those used for the Sperling and Sondhi model. See legend of Fig. 9. The subtraction, static nonlinearity, and criterion ΔRs were identical to that used with the first merged model. See legend of Fig. 17.

the static nonlinearity to Sperling and Sondhi's model. As shown in Fig. 18(A), we inserted them before the final low-pass filter since we knew from simulations of MUSNOL that low-pass filtering after the static nonlinearity is necessary to predict the background-onset effect (see earlier discussion of Geisler fix).

As can be seen in Fig. 18(B), the amplitude-sensitivity vs frequency curves predicted by this second merged model are much closer together at the high-frequency end than at the low-frequency end, that is, they show high-frequency linearity. Further, as shown in Fig. 18(C), this second merged model does successfully predict a background-onset effect. Thus, qualitatively at least, this second merged model can predict the phenomena from both traditions.

DISCUSSION

The merged models that can predict the phenomena from both traditions contain four parts: (1) a frequency-dependent gain-controlling process as in the periodic-tradition model; (2) a subtractive process as in the aperiodic-tradition model; (3) a static nonlinearity that follows the subtractive process as in the aperiodic-tradition model; and (4) more low-pass filtering as in both traditions' models. While not being able to claim that all four of the parts are essential, or that the ordering must be exactly as specified above, we have discovered that many other combinations of the component parts from the periodic-tradition and aperiodic-tradition models will not predict the two phenomena discussed here: high-temporal-frequency linearity and the background-onset effect.

None of the parts of the merged models, however, is necessarily correct in detail. Many modifications or substitutes would clearly work just as well at this qualitative level. For example, rather than the feedback or feedback–feedforward gain-changing modules used at the front end of the models in Figs 17 and 18, one might use a module incorporating one of Tranchina and Peskin's (1988) wiring diagrams. Also, one could certainly expand the model to include more parts. For example, some investigators talk of more than one subtractive process (one slower and one faster, e.g. Hayhoe, 1990). Similarly, the initial gain-controlling process might be composed of several processes having somewhat different properties; for example, one process might change the time-constant of the impulse–response but leave unchanged the area underneath it (the gain) while another process might affect the height of the impulse–response (and thus the gain) while leaving the time-constant unaltered (e.g. pigment depletion at very high luminances). Conversely, two of the above parts could be combined; in principle, for example, the subtractive process and the gain-changing process could probably be combined into a unitary process.

While both the merged models described above are able to qualitatively predict the two phenomena focussed on here, no attempt was made to fine-tune either model to predict all the details in any one set of psychophysical data (e.g. Figs 1 and 5), much less in all the other psychophysical results that such a model might bear on (e.g. the background-*offset* effect, systematically varying the SOA between the background and the test, detection thresholds for various kinds of aperiodic stimuli, experiments using combinations of periodic and aperiodic stimuli). To attempt such a project in the future might be worthwhile, particularly if the experimental results were all collected on the same subjects using the same psychophysical methods and stimuli identical on the dimensions not under consideration (spatial dimensions and wavelength).

Physiological correlations. It is premature to discuss at any length the possible physiological substrates for these processes; at this point there are many pieces of knowledge but few definitive conclusions. However, the output of retinal ganglion cells in response to sinusoidally-flickering lights shows a strong interaction between temporal frequency and mean luminance quite similar to human psychophysics (Lee, Pokorny, Smith, Martin & Valberg, 1990; Purpura, Tranchina, Kaplan & Shapley, 1990). Probably, therefore, the front end gain-changing process of the model occurs at the retinal level in the primate. The subtractive and static nonlinear stages might come later than the retina, although at this point one cannot rule out the possibility that they also occur in the retina. The placement of the extra low-pass filtering (the fourth part of the merged models listed above) is arbitrary, and it seems likely to be distributed throughout retinal and later processing. [See Hayhoe (1990) for further discussion of the physiological substrate as well as its possible connection to the early nonlinearities recently described by Pelli (1986) and MacLeod, Williams and Makous (1992).]

Noise and decision rules

There are a number of ways in which the assumptions of the merged models are too limited and might be extended. Here we discuss two: (1) The merged models are deterministic, that is, they contain no explicit probabilistic processes. However, there is noise (variability) both in physiological results and psychophysical results. Indeed, this noise is often taken to be the limiting factor that determines thresholds (see discussions in, e.g. Cohn & Lasley, 1986; Geisler, 1989; Graham, 1989). (2) It would be naive to assume that any particular simple decision rule, like the constant-ΔR rule used above, is a good description of all the processing that occurs at higher levels in the nervous system, except perhaps in very limited circumstances.

Quantal noise. Quantal noise exists in the visual stimulus, as is well known (see Pelli, 1990, for a current discussion). Should this quantal noise be included explicitly in models of light adaptation dynamics? Our current answer is a cautious no, as we discuss at some length in Graham and Hood (1992). Quantal noise seems rarely to be a limiting factor, nor can it straightforwardly explain the effects of light adaptation it is often called upon to explain. Hayhoe (1990) also believes that quantal noise need not be explicitly included. Her reasoning is that the noise can be subsumed in the final static nonlinearity unless that nonlinearity changes with adaptation state. The success of these models suggests it does not.

Multiplicative late noise and the $\Delta R/R$ rule. Late noise can be at least approximately multiplicative (increasing as response magnitude increases). The variance of cortical neurons, for example, increases as the mean increases (Dean, 1981; Tolhurst, Movshon & Thompson, 1981). If late noise is approximately multiplicative, then, whenever there is a transient peak at the onset of a step–response, most models will predict a transient increase in increment threshold at that onset. Rather than modeling this multiplicative noise directly, one can approximate its effects by using the following constant-ratio rule (see, e.g. Matin, 1968) as an alternative for the constant-ΔR rule of equation (7). In any case, this seems a reasonable alternative rule to consider. In particular, at threshold,

$$\max_t [\Delta R(t)/R(t)] = \delta. \tag{9}$$

In models like that of Sperling and Sondhi (1968), the peak of the transient response at the onset of a stimulus is indeed greater than the steady-state response, that is, $R(t)$ is greater at onset than later. We asked whether this transient response coupled with the constant-ratio rule could predict the background-onset effect. Thus, we computed some predictions from Sperling and Sondhi's model with the constant-ratio decision rule of equation (9). Although there was a slight threshold elevation at some mean luminances for low SOAs relative to SOA = ∞, the effect was much less marked than the background-onset effect (Fig. 1). This failure to predict correctly the background-onset effect probably comes from the fact that the peak/steady-state ratio is not large in models like those of Sperling and Sondhi's. (A similar explanation was put forth above for the failure to repair Sperling and Sondhi's model by simply adding a static nonlinearity.)

Probability summation across time and Minkowski metrics (Quick Pooling Formula). If a response is noisy, there will be "probability summation across time" (as well as across other dimensions). Rather than explicitly including noise in the model of the response, however, one can sometimes use a deterministic model of the response and calculate these probability-summation effects (see, e.g. Graham, 1989; Quick, 1974; Watson, 1986). A more complicated decision rule than the constant-response or constant-ratio decision rules used here is needed. In particular, the appropriate measure of response at each moment in time is raised to some power (usually in the range 3–5) and then integrated across time. This kind of computation is sometimes referred to as the Quick Pooling Formula or the use of a Minkowski metric. It is relatively straightforward to justify (as an approximation to a model with noise) in the case of simple detection, that is, when a stimulus eliciting a

non-baseline average response is being discriminated from a stimulus eliciting a baseline response. The thresholds for sinusoidal flickering stimuli and, to a lesser extent, for an aperiodic test probe at an SOA = ∞ might be viewed as examples of simple detection. But the threshold for the aperiodic test probe at SOA = 0 is clearly not (see further discussion below). On the other hand, some variant of this computation might serve as an alternative decision rule. It seems unlikely to alter any of our basic conclusions, however. All four parts of the merged model would still need to be included.

Yet more complicated decision rules and higher-level processing. In an experiment where an aperiodic test probe stimulus is superimposed on a background a discrimination is made between two suprathreshold stimuli, that is between two stimuli which are themselves each discriminable from a blank. One is the background alone and the other is the background plus test probe. In fact, the SOA = 0 resembles a masking paradigm where the background onset is the masking stimulus and the test probe is the test stimulus. This suggests thinking of the threshold elevation at SOA = 0 as due to "masking". In a way, this is just using one phenomenon's name to label another similar one, but it does suggest to some people that it should be explained with a $\Delta R/R$ decision rule or multiplicative noise (without the subtractive and static nonlinearity stages). However, as we saw above, this possibility can be ruled out.

The more vaguely-stated possibility suggested by this observation, however, is that any decision rule of the kind considered above may be in principle inadequate for the suprathreshold-discrimination case. It may be impossible to explain suprathreshold discriminations without more explicit modeling of higher-level visual processes than is necessary to explain detection (where detection is a discrimination between a stimulus and a neutral stimulus). In the suprathreshold discrimination case, the observer is trying to discriminate between two sets of neural responses (the set in response to stimulus A vs the set in response to stimulus B), both of which sets contain many non-baseline responses. In the detection case, on the other hand, the observer is simply trying to detect some non-baseline response in either set (since that is the set most likely to be the non-blank stimulus). Thus a simple decision rule may be suitable in the detection case simply because all the higher-level processes are reduced to such simple action that they become transparent. But no such simple decision rule may ever be discovered for a suprathreshold case (see a similar discussion in Graham, 1989, pp. 12 and 309 for the case of spatial vision). Bowen (1989) makes a similar argument for a three-flash experiment.

However, at this moment in time, we seem to be able to explain the background-onset effect with a subtractive process and a static nonlinearity. Thus, we can just leave as a marker for the future—should troubles in fully explaining the data arise—the possibility that the background-onset effect in particular (and perhaps all the results) will not be explained in detail without including more about higher-level visual processing.

Spatial models from periodic-stimulus tradition—multiple channels and the constant-flux hypothesis

In addition to pointing out the empirical relationship that describes the interaction between spatial or temporal frequency and transition luminance (Fig. 6), van Nes and Bouman (1967) suggested a possible mechanism to explain this relationship. For the spatial case, elaborated forms of this mechanism appear in Shapley and Enroth-Cugell (1984) as the "channels" hypothesis and in Chap. 13 of Graham (1989) as the "constant-flux" hypothesis. This mechanism suggested for the spatial case is very different from the processes suggested for the temporal case in dynamic models of light adaptation like those we have been discussing.

This mechanism for the spatial case relies on the existence of different spatial-frequency channels with different sizes of receptive field and with each showing a transition (e.g. that between the de Vries–Rose and Weber regions) at a constant flux and, therefore, at a different mean luminance. (Flux is luminance summed over the receptive field's excitatory center.) In the spatial case, as much physiological and psychophysical evidence has confirmed, different sizes of receptive field are presumably involved in the detection of different spatial frequencies with at least 7 or 8 different sizes serving any one retinal position. Physiological evidence for the constant-flux hypothesis about transition luminances has also been reported (Shapley & Enroth-Cugell, 1984). The value of this multiple-channel, constant-flux idea remains to be determined, however. Problems occur in attempting to generalize it across retinal position (see Graham, 1989, Chap. 13) and there is at least one competing hypothesis for spatial vision (Chen, MacLeod & Stockman, 1987).

Since the interaction of temporal frequency with mean luminance is much like that of spatial frequency, it is tempting to develop an analogous explanation. Psychophysical evidence, however, strongly suggests that temporal-frequency channels are much more broadly tuned than spatial-frequency channels, so broadly that there are effectively only two or three of them across the whole temporal-frequency range at any constant spatial frequency (see e.g. Graham, 1989, Chap. 12). This seems an insufficient number to explain the dramatic and apparently continuous change in temporal transition luminance that occurs with change in temporal frequency. To put it another way, although psychophysical contrast sensitivity functions of spatial frequency and of temporal frequency are very similar and change similarly with mean luminance, the processes acting on the two dimensions are probably quite dissimilar. The multiple-channel, constant-flux hypothesis is tenable only for the spatial-frequency case. A different kind of explanation (e.g. the one embodied in the above dynamic models of light adaptation) probably needs to be found for the temporal-frequency case. Consistent with this suggestion, temporal properties of individual striate cortical neurons are affected by mean luminance in much the same way as are psychophysical results (e.g. Fig. 5 here),

but the spatial properties are affected little if at all (Kaufman & Palmer, 1990).

CONCLUSION

Although the merged models are successful at capturing the two important phenomena that the original models failed to describe, they have not been fine-tuned to account in quantitative detail for any particular set of flicker-sensitivity or background-onset effect results nor to account for other psychophysical results such models might bear on. Undoubtedly the parameters and perhaps other characteristics of the merged models' components will be modified in the future. It seems likely, however, that future models of the dynamics of light adaptation will need to contain the basic features of these merged models.

REFERENCES

Adelson, E. H. (1982). Saturation and adaptation in the rod system. *Vision Research, 22,* 1299–1312.

Alpern, M., Rushton, W. A. H. & Torii, S. (1970). Signals from cones. *Journal of Physiology, 207,* 463–475.

Baker, H. D. (1949). The course of foveal light adaptation measured by the threshold intensity increment. *Journal of the Optical Society of America, 39,* 172–179.

Baylor, D. A., Hodgekin, A. L. & Lamb, T. D. (1974). Reconstruction of the electrical responses of turtle cones to flashes and steps of light. *Journal of Physiology, 242,* 759–791.

Bouguer (1760). *Traite d'Optique sur la gradation de la Lumiere.* Paris.

Bowen, R. (1989). Two pulses seen as three flashes. *Vision Research, 29,* 409–417.

Boynton, R. M. & Kandell, G. (1957). On responses in the human visual system as a function of adaptation level. *Journal of the Optical Society of America, 47,* 275–286.

Boynton, R. M. & Whitten, D. N. (1970). Visual adaptation in monkey cones: Recordings of late receptor potentials. *Science, 170,* 1423–1426.

Chen, B., MacLeod, D. I. A. & Stockman, A. (1987). Improvement in human vision under bright light: Grain or gain? *Journal of Physiology, 394,* 41–66.

Cohn, T. E. & Lasley, D. J. (1986). Visual sensitivity. *Annual Review of Psychology, 37,* 495–521.

Craik, K. J. (1938). The effect of adaptation on differential brightness discrimination. *Journal of Physiology, 92,* 406–421.

Crawford, B. H. (1947). Visual adaptation in relation to brief conditioning stimuli. *Proceedings of the Royal Society B, 134,* 283–302.

Dean, A. F. (1981). The variability of discharge of simple cells in the cat striate cortex. *Experimental Brain Research, 44,* 437–440.

Dodge, F. A., Knight, B. W. & Toyoda, J. (1968). Voltage noise in *Limulus* visual cells. *Science, 160,* 88–90.

van Essen, D. C. (1985). Functional organization of primate visual cortex. In Jones, E. G. & Peters, A. (Eds), *Cerebral cortex* (Vol. 3, pp. 259–329). New York: Plenum Press.

Finkelstein, M. A. & Hood, D. C. (1981). Cone system saturation: More than one stage of sensitivity loss. *Vision Research, 21,* 319–328.

Finkelstein, M. A., Harrison, M. & Hood, D. C. (1990). Sites of sensitivity control within a long-wavelength cone pathway. *Vision Research, 30,* 1145–1158.

Fuortes, M. G. F. & Hodgekin, A. L. (1964). Changes in time scale and sensitivity in the ommatidia of *Limulus*. *Journal of Physiology, 172,* 239.

Geisler, W. S. (1978). Adaptation, afterimages, and cone saturation. *Vision Research, 18,* 279–289.

Geisler, W. S. (1979). Initial image and afterimage discrimination in the human rod and cone systems. *Journal of Physiology, 294,* 165–179.

Geisler, W. S. (1981). Effects of bleaching and backgrounds on the flash response of the cone system. *Journal of Physiology, 312,* 413–434.

Geisler, W. S. (1983). Mechanisms of visual sensitivity: Backgrounds and early dark adaptation. *Vision Research, 23,* 1423–1432.

Geisler, W. S. (1989). Sequential ideal-observer analysis of visual discriminations. *Psychological Review, 96,* 267–314.

Graham, N. (1989). *Visual pattern analyzers.* New York: Oxford University Press.

Graham, N. & Hood, D. (1989). Comparison of adaptation studies using periodic and aperiodic stimuli. Invited paper at the Annual Meeting of the Optical Society of America, 15–20 October 1989, Orlando, Fla.

Graham, N. & Hood, D. (1992). Quantal noise and decision rules in dynamic models of light adaptation. *Vision Research. 32,* 779–787.

Hayhoe, M. M. (1990). Spatial interactions and models of adaptation. *Vision Research, 30,* 957–965.

Hayhoe, M. M., Benimoff, N. I. & Hood, D. C. (1987). The time course of multiplicative and subtractive adaptation proces. *Vision Research, 27,* 1981–1996.

Hess, R. F. & Nordby, K. (1986). Spatial and temporal limits of vision in the achromat. *Journal of Physiology, 371,* 365–385.

Hood, D. C. (1978). Psychophysical and electrophysiological tests of physiological proposals of light adaptation. In Armington, J., Krauskopf, J. & Wooten, B. (Ed.), *Visual psychophysics: Its physiological basis* (pp. 141–155). London: Academic Press.

Hood, D. C. & Finkelstein, M. A. (1986). Sensitivity to light. In Boff, K., Kaufman, L. & Thomas, J. (Eds), *Handbook of perception and human performance* (Chap. 5). New York: Wiley.

Hood, D. C. & Greenstein, V. C. (1982). An approach to testing alternative hypothesis of changes in visual sensitivity due to retinal disease. *Investigative Ophthalmology and Visual Science, 23,* 96–101.

Hood, D. C. & Greenstein, V. (1990). Models of the normal and abnormal rod system. *Vision Research, 30,* 51–68.

Hood, D. C., Finkelstein, M. A. & Buckingham, E. (1979). Psychophysical tests of models of the response–intensity function. *Vision Research, 19,* 401–406.

Hood, D. C., Ilves, T., Maurer, E., Wandell, B. & Buckingham, E. (1978). Human cone saturation as a function of ambient intensity: A test of models of shifts in the dynamic range. *Vision Research, 18,* 983–993.

Hurvich, L. M. & Jameson, D. (1958). Further development of a quantified opponent-color theory. In *Vision problems of color II* (pp. 691–723). London: HMSO.

Jameson, D. & Hurvich, L. M. (1972). Color adaptation: Sensitivity control, contrast, after-images. In Jameson, D. & Murvich, L. M. (Eds) *Handbook of sensory physiology* (pp. 568–581). Berlin: Springer.

Kaufman, D. A. & Palmer, L. A. (1990). The luminance dependence of spatiotemporal response of cat striate cortical units. *Investigative Ophthalmology and Visual Science, 314,* 398.

Kelly, D. H. (1961). Visual responses to time-dependent stimuli. II. Single-channel model of the photopic visual system. *Journal of the Optical Society of America, 51,* 747–754.

Kelly, D. H. (1972). Adaptation effects on spatio-temporal sine-wave thresholds. *Vision Research, 12,* 89–101.

Landy, M. & Movshon, A. J. (1992). *Computational models of visual processing.* Cambridge, Mass. MIT Press.

de Lange, H. (1952). Experiments on flicker and some calculations on an electrical analogue of the fovea. *Physica, 28,* 935–950.

de Lange, H. (1954). Relationship between critical flicker-frequency and a set of low-frequency characteristics of the eye. *Journal of the Optical Society of America, 44,* 380–389.

de Lange, H. (1958). Research into the dynamic nature of the human fovea-cortex systems with intermittent and modulated light. *Journal of the Optical Society of America, 48,* 771–789.

Lee, B. B., Pokorny, J., Smith, V. C., Martin, P. R. & Valberg, A. (1990). Luminance and chromatic modulation sensitivity of macaque ganglion cells and human observers. *Journal of the Optical Society of America A, 7,* 2223–2237.

LeGrand, Y. (1957). *Light, color and vision.* London: Chapman & Hall.

MacLeod, D. I. A. (1978). Visual sensitivity. *Annual Review of Psychology, 29,* 613–645.

MacLeod, D. I. A., Williams, D. R. & Makous, W. (1992). A visual nonlinearity fed by single cones. *Visual Science.* In press.

Matin, L. (1968). Critical duration, the differential luminance threshold, critical flicker frequency, and visual adaptation: A theoretical treatment. *Journal of the Optical Society of America, 58,* 404–415.

van Nes, F. L. (1968). Experimental studies in spatiotemporal contrast transfer by the human eye. Ph.D. thesis, University of Utrecht, The Netherlands.

van Nes, F. L. & Bouman, M. A. (1967). Spatial modulation transfer in the human eye. *Journal of the Optical Society of America, 57,* 401–406.

van Nes, F. L., Koenderink, J. J., Nas, H. & Bouman, M. A. (1967). Spatiotemporal modulation transfer in the human eye. *Journal of the Optical Society of America, 57,* 1082–1088.

Pelli, D. (1986). Bright areas appear magnified: A visual saturation? *Investigative Ophthalmology and Visual Science (Suppl.) 31,* 494.

Pelli, D. (1990). The quantum efficiency of vision. In Blakemore, C. (Ed.), *Vision: Coding and efficiency.* Cambridge: Cambridge University Press.

Purpura, K., Tranchina, D., Kaplan, E. & Shapley, R. M. (1990). Light adaptation in the primate retina: Analysis of changes in gain and dynamics of monkey retinal ganglion cells. *Visual Neuroscience, 4,* 75–93.

Quick, R. F. (1974). A vector-magnitude model of contrast detection. *Kybernetik, 16,* 65–67.

Robson, J. G. & Graham, N. (1981). Probability summation and regional variations in sensitivity across the visual field. *Vision Research, 21,* 409–418.

Rose, A. (1942). The relative sensitivities of television pick-up tubes, photographic film, and the human eye. *Proceedings of the Institute of Radio Engineers, 30,* 295–300.

Rose, A. (1948). The sensitivity performance of the human eye on an absolute scale. *Journal of the Optical Society of America, 38,* 196–208.

Rovamo, J. & Raninen, A. (1988). Critical flicker frequency as a function of stimulus area and luminance at various eccentricities in human cone vision: A revision of Granit–Harper and Ferry–Porter laws. *Vision Research, 28,* 785–790.

Shapley, R. M. & Enroth-Cugell, C. (1984). Visual adaptation and retinal gain controls. In Osborne, N. N. & Chader, G. J. (Eds), *Progress in retinal research* (Vol. 3, pp. 263–343). Oxford: Pergamon Press.

Shevell, S. K. (1977). Saturation in human cones. *Vision Research, 17,* 427–434.

Shevell, S. K. (1978). The dual role of chromatic backgrounds in color perception. *Vision Research, 18,* 1649–1661.

Sperling, G. (1989). Three stages and two systems of visual processing. *Spatial Vision, 4,* 183–207.

Sperling, G. & Sondhi, M. M. (1968). Model for visual luminance discrimination and flicker detection. *Journal of the Optical Society of America, 58,* 1133–1145.

Stiles, W. S. (1959). Color vision: The approach through increment threshold sensitivity. *Proceedings of the National Academy of Sciences, U.S.A., 45,* 100–114.

Tolhurst, D. J., Movshon, J. A. & Thompson, I. D. (1981). The dependence of response amplitude and variance of cat visual cortical neurons on stimulus contrast. *Experimental Brain Research, 41,* 414–419.

Tranchina, D. & Peskin, C. S. (1988). Light adaptation in the turtle retina: Embedding a parametric family of linear models in a single nonlinear model. *Visual Neuroscience, 1,* 339–348.

Tranchina, D., Gordon, J. & Shapley, R. M. (1984). Retinal light adaptation—evidence for a feedback mechanism. *Nature, 310,* 314–316.

Tyler, C. W. & Hamer, R. D. (1990). Analysis of visual modulation sensitivity. IV. Validity of the Ferry–Porter law. *Journal of Optical Society of Ameerica A, 7,* 743–758.

de Vries, H. (1942). The quantum character of light and its bearing upon the threshold of vision, the differential sensitivity and visual acuity of the eye. *Physica, 10,* 553.

Walraven, J. (1976). Discounting the background—the missing link in the explanation of chromatic induction. *Vision Research, 16,* 289–295.

Walraven, J. & Valeton, J. M. (1984). Visual adaptation and response saturation. In Van Doorn, A. J., Van de Grind, W. A. & Koenderink, J. J. (Eds), *Limits in perception.* Utrecht: VNU Science Press.

Watson, A. B. (1986). Temporal sensitivity. In Boff, K., Kaufman, L. & Thomas, J. (Eds), *Handbook of perception and human performance* (Chap. 6). New York: Wiley.

Acknowledgements—This research was supported by National Eye Institute Grants EY-08459 and EY-02115.

APPENDIX

Details of Model Predictions

The calculations were programmed using MATLAB (from Math Works Inc.—on a Macintosh IIci). All the predictions can be calculated using the three different kinds of modules for which equations are given below: a linear low-pass module (a case of exponential filters), a feedback module, and a feedforward module.

The predictions were calculated incrementally across time using difference-equation approximations to differential equations. (The differential equations can be found, e.g. in Sperling & Sondhi, 1968.) In the equations below i indexes the discrete time steps, and Δt is the length of each discrete time step. In the predictions shown here, Δt was equal to 0.5 msec for the flickering stimuli and for the MUSNOL's response to the aperiodic stimuli; it equaled 0.1 msec for the first merged model's response to the aperiodic stimuli; and it equaled 0.05 msec for the Sperling and Sondhi model's and for the second merged model's response to aperiodic stimuli. We ensured that the time sampling used here was adequate by checking that further decreases in Δt did not affect the predictions.

For the predictions involving flickering stimuli, we checked that the responses of the models had settled down before the interval over which $\max \Delta R(t)$ was computed (to avoid transient effects due to the onset or the mean luminance or of the flicker). For predictions involving aperiodic stimuli, we checked that the whole response to the test was included in the interval we considered.

Some other parameters values for the modules are given as examples below but most are in the figure legends.

It may be useful to point out that the three equations below—those for the linear, the feedback, and the feedforward modules—are very similar, differing only in the quantity that multiplies $f_j(i-1)$ at the far right side; this quantity is 1 for the linear case and incorporates the feedback and feedforward control signals in the other cases.

Linear lowpass module (cascaded exponential filters)

The linear low-pass module considered here contains n stages, each of which is an exponential filter. This module is illustrated in Fig. 7. The equation for each stage of exponential filtering is

$$f_j(i) = f_j(i-1) + (\Delta t/\tau)\cdot[f_{j-1}(i-1) - f_j(i-1)]$$

where n is the total number of exponential-filtering stages; $f_j(i)$ (for $j = 1$–n) is the response of the jth stage at the ith time step [so $f_n(i)$ is the output of the whole module at the ith time step]; $f_o(i)$ is the input to the low-pass module (e.g. the left column in Fig. 7, or the output from the feedforward module in the model of Sperling and Sondhi of Figs 8, 9 and 12) at the ith time step; and τ is the time constant of each stage.

In MUSNOL the low-pass modules LP_1, LP_D, LP_M, and LP_S, are all cascades of stages of exponential filters and described by the above equation. See the legend of Fig. 15 for parameters. In the Sperling and Sondhi model and in the merged models, there is a final low-pass module containing six stages ($n = 6$) each having a time constant of 6 msec ($\tau = 6$).

Feedback module equation

The equation for each stage of feedback was

$$f_j(i) = f_j(i-1) + (\Delta t/\tau)\cdot\{f_{j-1}(i-1) - f_j(i-1)\cdot[1 + g\cdot f_n(i-1)]\}$$

where n is the total number of feedback stages; $f_j(i)$ (for $j = 1$–n) is the response of the jth feedback stage at the ith time step [so $f_n(i)$ is the output of the whole feedback module at the ith time step]; $f_o(i)$ is the input to the feedback module (which is the stimulus in all the models considered here) at the ith time step; τ is the time constant of each feedback stage; and g is the strength of the feedback from the last stage's output to each preceding stage and was always set equal to 1.0 in the calculations reported here.

In the Sperling and Sondhi model (Figs 8, 9 and 12) which was also incorporated in the second merged model (Fig. 18), there was an initial feedback module that had two stages ($n = 2$) and the time-constant of each stage (τ) was 20 msec. In the first merged model (Fig. 17), the feedback module contained four stages ($n = 4$) where the time-constant of each stage (τ) was 20 msec.

Feedforward module equation

In the feedforward module of the Sperling and Sondhi model, there was only one stage ($n = 1$). The equation for the main path through this stage ($j = 1$) was

$$f_j(i) = f_j(i-1) + (\Delta t/\tau)\cdot\{f_{j-1}(i-1) - f_j(i-1)\cdot[1 + f_D(i-1)]\}$$

where $f_1(i)$ is the response of the one feedforward stage (and hence the output of the feedforward module) at the ith time step; $f_o(i)$ is the input to the feedforward module (which is the output of a feedback module in all the models considered here) at the ith time step; τ is the time constant of each feedforward stage; and $f_D(i)$ is the delayed control signal at the ith time step.

In the model of Sperling and Sondhi (Figs 8, 9 and 12 and incorporated in the second merged model, Fig. 18), the delayed control signal was the output of one stage of linear exponential filtering (as in the first equation of this Appendix).